Ripening of porous media

Benny Davidovitch,* Deniz Ertaş, and Thomas C. Halsey
Corporate Strategic Research, ExxonMobil Research and Engineering, 1545 Route 22 East, Annandale, New Jersey 08801, USA
(Received 26 April 2004; published 30 September 2004)

We address the surface-tension-driven dynamics of porous media in nearly saturated pore-space solutions. We linearize this dynamics in the reaction-limited regime near its fixed points—surfaces of constant mean curvature (CMC surfaces). We prove that the only stable interface for this dynamics is the plane and estimate the time scale for a CMC surface to become unstable. We also discuss the differences between dynamics in open and closed environments, pointing out the unlikelihood that CMC surfaces are ever realized in such environments on any time scale.

DOI: 10.1103/PhysRevE.70.031609 PACS number(s): 61.43.Gt, 47.54.+r, 47.70.−n

I. INTRODUCTION

When solid grains are suspended in a solution saturated with the molecular constituents of the grains, they undergo coarsening under the thermodynamic driving force of surface tension. During this phenomenon, known as Ostwald ripening, the free energy of the system is lowered by minimizing the contact area between the coexisting phases. Molecules dissolve from high-curvature areas of the interface, pass through the solution, and can precipitate in low-curvature surface regions. This dynamics can be very complicated and depends on many parameters such as chemical composition, induced temperature and pressure fields, and other factors [1].

For the case of grains suspended in a solution, a mean field theory due to Lifshitz-Slyozov and Wagner is successful in capturing the dynamics at late stages of the ripening process for low solid volume fraction [2]. Another example of surface-tension-driven ripening arises in the kinetics of foams [3], in which the passage of gas across the fluid borders separating gas bubbles allows larger bubbles to grow at the expense of smaller ones—dry foams with a small liquid volume fraction represent an opposite limit from the Lifshitz-Slyozov-Wagner case.

In this report we study Ostwald ripening in porous media, where the fluid in the pore space is approximately saturated with the ingredients of the solid phase. Unlike the examples above, in typical porous media both the solid and pore space components of the medium are connected. An example would be a sedimentary material such as sandstone, with the water in the pore space saturated with the silica components of the rock. Another example would be crushed ice, with water vapor saturating the air in the pore space between ice grains.

It is clear that the fixed points of the dissolution-precipitation dynamics are surfaces of "constant mean curvature" (CMC surfaces). However, determining whether such surfaces are metastable or unstable is considerably more involved than in the case of isolated spheres discussed above. We are able to show that arbitrary surfaces are unstable to Ostwald ripening under a quite general set of circumstances, a fact which may have implications for the ultimate fate of bicontinuous porous media in geophysical and other applications. We are unaware of any previous demonstration of this fundamental property of two-component systems that attains the level of generality of our discussion.

While we are able to estimate time scales for these instabilities for geophysical systems, for real earth science systems dissolution-precipitation dynamics involve complicated multicomponent equilibria, and non-surface-tension-related mechanisms such as pressure solution often dominate as well [4].

II. EQUATIONS OF SURFACE MOTION

Following [5] we consider the evolution of an interface $\Gamma \equiv \mathbf{x}(u,v)$ between a porous, single component, isotropic solid and its ideal solution in the interstitial fluid. The solid is subject to a first order dissolution-precipitation reaction in a flow field of velocity $\mathbf{v}$. The normal velocity of the surface $u_n(\mathbf{x})$ into the pore space is given by

$$u_n(\mathbf{x}) = -K_f(1 - e^{-\Delta\mu(\mathbf{x})/kT}), \tag{1}$$

where K_f is the dissolution rate, and the precipitation rate is controlled by the Boltzmann factor associated with the difference $\Delta\mu(\mathbf{x}) \equiv \mu_{\mathrm{sur}}(\mathbf{x}) - \mu_{\mathrm{sol}}(\mathbf{x})$ between the chemical potentials of solid and dissolved molecules at the interface Γ. Referred to the chemical potential μ_{flat} for a flat surface in equilibrium with an ideal saturated solution of concentration c_{sat}, these are given by

$$\mu_{\mathrm{sur}}(\mathbf{x}) = \mu_{\mathrm{flat}} + 2\nu_m \sigma H(\mathbf{x}), \tag{2}$$

$$\mu_{\mathrm{sol}}(\mathbf{x}) = \mu_{\mathrm{flat}} + kT \ln\frac{c(\mathbf{x})}{c_{\mathrm{sat}}}, \tag{3}$$

where ν_m is the molecular volume in the solid, σ is the interfacial energy, $c(\mathbf{x})$ is the concentration near the surface point $\mathbf{x}$, and $H(\mathbf{x}) \equiv (1/2)(\delta S/\delta V)$ is the mean curvature, which measures the local variation in surface area δS with respect to a volume change δV of the solid. Here and elsewhere we define all concentrations with respect to the concentration in the solid.

*Present address: Division of Engineering and Applied Sciences, Harvard University, Cambridge, MA 02138, USA.

 ©2004 The American Physical Society

For $\Delta\mu \ll kT$, Eq. (1) reduces to

$$u_n(\mathbf{x}) = -K_f \frac{2\nu_m\sigma}{kT}\left[H(\mathbf{x}) - \frac{kT}{2\nu_m\sigma}\ln\frac{c(\mathbf{x},t)}{c_{\text{sat}}}\right]. \tag{4}$$

Since H should be no larger than the inverse of a typical pore size L, and $\nu_m\sigma/kT$ is usually a molecular scale

$$\frac{kT}{\nu_m\sigma} \gg L^{-1} \geqslant H, \tag{5}$$

we see that the linearized form of the dynamics holds for a nearly saturated solution $c \approx c_{\text{sat}}$.

The surface dynamics described in Eq. (4) depends on the dynamics of the concentration field $c(\mathbf{x},t)$ in the solution, which in turn is determined by an advection-diffusion equation,

$$\frac{\partial c}{\partial t} = -\nabla\cdot\mathbf{J} = D\nabla^2 c - \nabla\cdot(\mathbf{v}c), \tag{6}$$

$$J_n(\mathbf{x}) = \frac{1}{\nu_m}u_n(\mathbf{x}) \text{for } \mathbf{x} \in \Gamma, \tag{7}$$

where $\mathbf{J}$ is the current, and J_n its component in the normal direction to the surface. D is the diffusion constant, and $\mathbf{v}$ is the fluid velocity, whose normal component v_n must vanish on Γ. Note that our use of Eq. (1) implies that the dissolution-reprecipitation process cannot be strongly transport limited; i.e., we are neglecting any dependence of K_f on c. Equation (7) expresses kinematic boundary conditions for Eq. (6) on Γ. Far from the evolving interface the solution concentration reaches some spatially homogeneous value, and the velocity $\mathbf{v}$ is given by the flow in the medium, which solves the appropriate fluid dynamical equation for the boundary conditions on fluid flow in the medium.

As already hinted, the nature of the problem we have to consider depends strongly on whether we are concerned with reaction-limited or transport-limited kinetics. The reaction rate K_f determines a typical reaction time $\tau_{\text{react}} \equiv L/K_f$. The transport time τ_{trans}, which appears implicitly in Eq. (4) through the term $c(\mathbf{x},t)$, is the typical time for the solution concentration to relax to a spatially homogeneous value by the transport process described in Eq. (6). In this study we will be concerned only with the case $\tau_{\text{react}} \gg \tau_{\text{trans}}$; we are not interested herein in transport-limited phenomena such as dendritic growth at the surface.

Even with this restriction, we must still specify something about the nature of the transport in order to clearly define our problem. Consider the Péclet number characterizing transport in the medium, $\text{Pe} = vL/D$, where v is the characteristic fluid velocity and L the pore size, which serves as a characteristic length scale in the medium. In the limit $\text{Pe} \to 0$, there is no flow in the medium, and the total amount of solid material (whether in matrix form or in solution) must be conserved. In the opposite limit, in which the velocity $v \to \infty$, we expect the concentration everywhere in the medium to be fixed by the concentration upstream, outside the region in which the interface is evolving.

Since the full solution of the transport equations in a porous medium is daunting, we concentrate on these two limiting cases of this problem, which we term "perfect open" and "perfect closed" systems. In a perfect open system, the velocity of the flow through the medium is considered sufficiently rapid that in effect each element of the surface is in contact with fluid whose concentration c of the solute is fixed by a distant reservoir. Thus $c(\mathbf{x},t) = c$ in Eq. (4) is fixed in this case. The other limit of a "perfect closed" system, in which $v = 0$, will be explored at the end of this report.

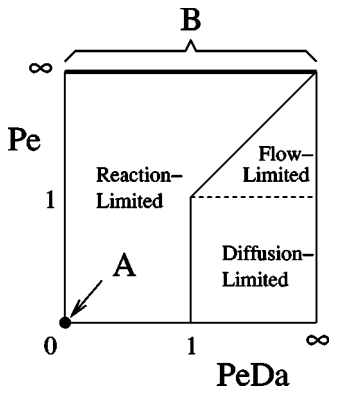

FIG. 1. Kinetic "phase diagram." Note that for low Pe the product PeDa determines whether the system is reaction-limited or transport limited, while for high Pe it is Da that determines this balance. Point A corresponds to a "perfect closed" system, while the line B (along which $\text{Da} = 0$) corresponds to a "perfect open" system.

Following Ref. [6], the various kinetic regimes are summarized in the "phase diagram" depicted in Fig. 1, as a function both of Pe as well as of the "Damköhler" number $\text{Da} = K_f/v$, which controls the degree of transport vs reaction limitation in the high-Péclet-number limit. In the low-Péclet-number limit, the degree of transport vs reaction limitation is controlled by the product of Pe and Da, as indicated in Fig. 1.

III. PERFECT OPEN SYSTEM: GEOMETRICAL FORMALISM

In the perfect open case, the concentration $c(\mathbf{x})$ on the solution side of the interface has the constant value c_∞, and the interface dynamics is governed only by Eq. (4), which yields

$$u_n(\mathbf{x}) = -K_f \frac{2\nu_m\sigma}{kT}[H(\mathbf{x}) - H^\star], \tag{8}$$

where $H_\star \equiv [kT/(2\nu_m\sigma)]\ln(c_\infty/c_{\text{sat}})$. The case $H^\star = 0$ corresponds to the well-known Allen-Cahn equation [1].

CMC surfaces, for which $H(\mathbf{x}) = H^\star$ everywhere on the surface, are the fixed points of the dynamics (8). These surfaces have been studied in a variety of contexts, notably for their relationship to certain phases of block copolymers [7]. The simplest examples are a sphere of radius $r = 1/H$ and a cylinder of radius $r = 1/2H$. We are more interested, however, in bicontinuous surfaces, in which the regions on both sides of the surface are connected; these will represent a better model for porous media, in which the solid matrix provides competence, while the fluid component is entirely connected allowing large-scale flows to occur.

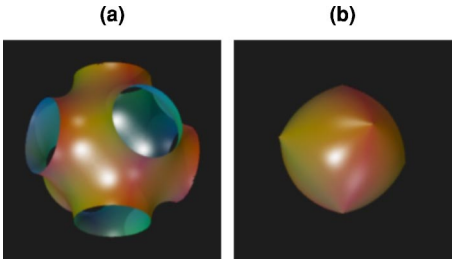

FIG. 2. (Color online) (a) The Schwartz *P* surface, a minimal (zero mean curvature) surface of simple cubic symmetry. A single unit cell is shown. (b) A single unit cell of size L of a CMC surface with $HL \approx 2.0$, which is close to a simple cubic lattice of touching spheres. Figures courtesy of J. T. Hoffman, MSRI Scientific Graphics Project, UC-Berkeley [8].

A special case of CMC surfaces are "minimal surfaces," for which $H(\mathbf{x})=0$. These surfaces have been extensively studied in the context of analytic function theory, and many such surfaces have been discovered, including bicontinuous surfaces, such as the famous triply periodic "Schwartz *P* surface" (see Fig. 2) [9]. For $H^\star=0$, Eq. (8) is the equation of motion for a manifold seeking to minimize its own surface area, a dynamics that is sometimes called "motion under mean curvature" [10].

Anderson *et al.* have extended several such surfaces into bicontinuous triply periodic CMC surfaces with $H\neq 0$ [11]. The extension of the Schwartz *P* surface to a family of CMC surfaces is shown in Fig. 3, with an example depicted in Fig. 2(b). These surfaces vary continuously from the *P* surface (M) to a simple cubic lattice of barely touching spheres at one end point (A), and to a simple cubic lattice of barely touching spherical holes at the other end point (A') (see Fig. 3). Anderson *et al.* also generated families corresponding to fcc, bcc, and diamond lattices of spheres, with qualitatively similar properties. Although we are aware of no reported examples of "amorphous" nonperiodic families of CMC surfaces, it is possible that such families exist. Such families would be most relevant to real porous media.

IV. STABILITY OF CMC SURFACES

We now show that all periodic CMC surfaces with the (degenerate) exception of planes are unstable fixed points of Eq. (8). Consider a surface $\mathbf{x}'(u,v)=\mathbf{x}+\epsilon(\mathbf{x})\mathbf{n}(\mathbf{x})$, whose deviation from a CMC surface $\mathbf{x}(u,v)\in\Gamma^\star$ with $H(\mathbf{x})=H^\star$ is given by a (small) normal displacement $\epsilon(\mathbf{x})$. In the Appendix we show that the corresponding variation $\delta H(\mathbf{x})=H(\mathbf{x}')-H^\star$ is given to first order in ϵ by

$$\delta H(\mathbf{x}) = -\left[((2H^\star)^2 - K)\epsilon + \nabla_s B\cdot\nabla_s\epsilon + \frac{1}{2}\nabla_s{}^2\epsilon\right], \quad (9)$$

$$B(\mathbf{x}) \equiv -\frac{1}{8}\ln[(H^\star)^2 - K(\mathbf{x})], \quad (10)$$

where ∇_s and ∇_s^2 are the surface gradient and Laplacian, respectively, and $K(\mathbf{x})$ is the Gaussian curvature at $\mathbf{x}$. Substituting Eq. (9) in Eq. (8), we obtain the linear dynamics near a CMC surface with mean curvature $H^\star$:

$$\frac{\partial\epsilon}{\partial t} = \frac{2K_f\nu_m\sigma}{kT}\mathcal{L}\epsilon, \quad (11)$$

$$\mathcal{L} \equiv 2(H^\star)^2 - K + \nabla_s B\cdot\nabla_s + \frac{1}{2}\nabla_s{}^2. \quad (12)$$

Recalling the definition of H and K in terms of the local principal radii of curvature of the surface R_1 and R_2,

$$H = (R_1^{-1}+R_2^{-1})/2, \quad K = (R_1R_2)^{-1}.$$

Since $2H^2-K=(R_1^{-2}+R_2^{-2})/2\geq 0$, uniform precipitation ($\epsilon>0$) decreases the mean curvature, making the surface locally more hospitable to deposition, while dissolution ($\epsilon<0$) increases the mean curvature, favoring further dissolution. This observation already suggests that the surface is likely to be unstable.

Because the term in $\mathcal{L}$ which couples Gaussian curvature gradients with the gradient of ϵ is non-Hermitian, it is more convenient to work with the Hermitian operator $\mathcal{H}$ defined via the "gauge transformation"

$$\mathcal{H} \equiv e^{B(\mathbf{x})}Le^{-B(\mathbf{x})} \quad (13)$$

so that

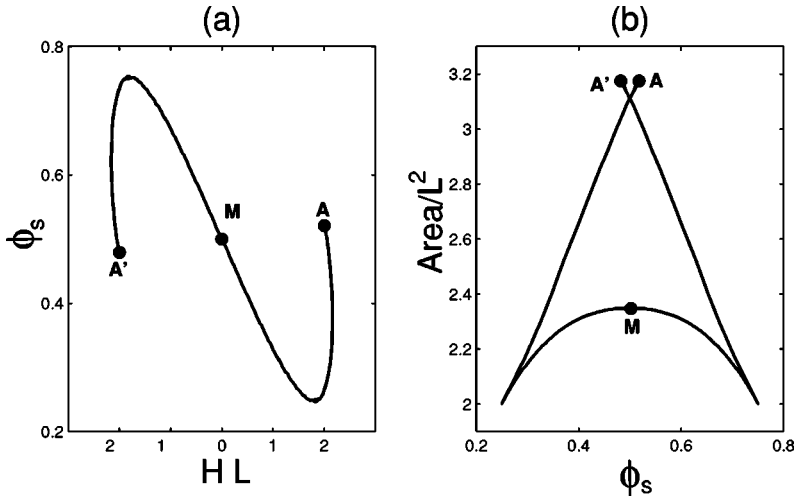

FIG. 3. (a) The dimensionless mean curvature HL versus ϕ_s, the solid volume fraction enclosed by the surface [Eq. (23)], for the constant mean curvature extension of the Schwartz *P* surface with unit cell size L. The minimal ($H=0$) *P* surface is represented by the point M, and the end points correspond to (A) a simple cubic lattice of touching spheres, and (A') a simple cubic lattice of touching spherical holes. (b) The surface area L^2 per unit cell of size L versus enclosed solid volume fraction ϕ_s for the same simple cubic CMC family. The lower branch is stable under periodic, volume-preserving, surface-minimizing dynamics. Figure adapted from Ref. [10], courtesy of *Advances in Chemical Physics*.

$$\mathcal{H} = V(\mathbf{x}) + \frac{1}{2}\boldsymbol{\nabla}_s{}^2, \tag{14}$$

$$V(\mathbf{x}) = (H^\star)^2 - K - \frac{1}{2}[\boldsymbol{\nabla}_s^2 B + (\boldsymbol{\nabla}_s B)^2]. \tag{15}$$

If the Hilbert spaces upon which the two operators $\mathcal{L}$ and $\mathcal{H}$ act are identical, the eigenvalues of $\mathcal{H}$ are identical to those of $\mathcal{L}$ [12]. This should certainly hold if we restrict ourselves to periodic surfaces. These eigenvalues are bounded from above provided that $|V(\mathbf{x})| < \infty$.

For any function $\Psi(\mathbf{x})$ defined on the surface, a lower bound on the maximum eigenvalue ω_0 of $\mathcal{H}$ (and consequently on the maximum eigenvalue of $\mathcal{L}$) can be established using the inequality

$$\omega_0 \geqslant \frac{\int_\Gamma dS \overline{\Psi}(H\Psi)}{\int_\Gamma dS|\Psi|^2}, \tag{16}$$

where $\int_\Gamma dS$ is the ordinary surface integral. Using the trial function $\Psi_B(\mathbf{x}) = e^{B(\mathbf{x})}$, we obtain

$$\omega_0 \geqslant \frac{\int_\Gamma dS[(H^\star)^2 - K]^{-1/4}[2(H^\star)^2 - K]}{\int_\Gamma dS[(H^\star)^2 - K]^{-1/4}}$$

$$= H_\star^2 + \frac{\int_\Gamma dS[(H^\star)^2 - K]^{3/4}}{\int_\Gamma dS[(H^\star)^2 - K]^{-1/4}}. \tag{17}$$

Note that $H^2 - K = [(1/R_1) - (1/R_2)]^2/4$ is non-negative everywhere on the surface, and reaches zero only at umbilic points of the surface for which $R_1 = R_2$. For minimal surfaces, these umbilics will be isolated points on the surface, while for more general CMC surfaces, we might expect them to be organized locally into arcs on the surface. Suppose that at a distance δ from the umbilic point we have $|R_1 - R_2| < A\delta^2$ (with A a constant) in the former case and $|R_1 - R_2| < A\delta$ in the latter case. It follows that the surface integral in the denominator on the right-hand side of Eq. (17) will not diverge, so that

$$\omega_0 > (H^\star)^2 \tag{18}$$

strictly.

Thus it follows that all CMC surfaces, porous or nonporous, are unstable to Ostwald ripening. This conclusion applies to periodic surfaces, but the structure of the argument strongly suggests that it will apply to nonperiodic (amorphous) CMC surfaces as well, should such surfaces exist.

For a system with a pore scale of L, we expect this instability to manifest itself on a time scale of

$$\tau_{\text{ripen}} = \omega_0^{-1} \sim \frac{kTL^2}{K_f \sigma \nu_m}. \tag{19}$$

Note that, intuitively, the instability is enhanced by an increase in the magnitude either of the mean curvature, or of the Gaussian curvature (since the latter is on average negative for a surface of large genus, such as a typical porous surface). In the sintering dynamics of "kissing" spheres, this dependence on the Gaussian curvature plays an important role [13].

For triply periodic CMC surfaces, the periodicity of the "potential" $V(\mathbf{x})$ implies that the eigenmodes $\Psi_{\mathbf{k},n}(\mathbf{x})$ of the operator $\mathcal{H}$ (and of $\mathcal{L}$) are surface Bloch functions,

$$\mathcal{H}\Psi_{\mathbf{k},n}(\mathbf{x}) = \omega_{\mathbf{k},n} e^{i\mathbf{k}\cdot\mathbf{x}} U_{\mathbf{k},n}(\mathbf{x}), \tag{20}$$

$$U_{\mathbf{k},n}(\mathbf{x}) = U_{\mathbf{k},n}(\mathbf{x} + \mathbf{R}), \tag{21}$$

where $\mathbf{R}$ is a lattice vector, $\mathbf{k}$ is the crystal momentum (confined to the first Brillouin zone), and n is a discrete label distinguishing between different branches. Standard techniques should allow determination of the spectrum of $\mathcal{H}$ throughout the first Brillouin zone.

Since the eigenfunction of the largest eigenvalue has the same sign (precipitation or dissolution) everywhere on the surface, the unstable dynamics of Eq. (8) involves transport of solute into (or out of) the pore space from the distant reservoir with fixed chemical potential.

V. CLOSED SYSTEM DYNAMICS

In a "perfect closed" system, the surface motion is reaction limited, such that the solute concentrations near the entire surface are equal to the average concentration in the pore $\overline{c}$. This condition is satisfied at the pore scale L if $D \gg K_f L/c_{\text{sat}}$. In addition, we impose conservation of total solid.

By integrating Eq. (4) over the surface, we see that $\overline{c}$ must then approach a value c_{eq} determined by

$$\ln\frac{c_{\text{eq}}(\overline{H})}{c_{\text{sat}}} = \frac{2\nu_m \sigma \overline{H}}{kT}, \tag{22}$$

controlled by the mean curvature $\overline{H}$ of the surface, over a characteristic time scale $\tau_{\text{pore}} = Lc_{\text{sat}}/K_f$. For $\tau > \tau_{\text{pore}}$, the solute concentration $\overline{c}$ is "slaved" to $c_{\text{eq}}(\overline{H})$. Conservation of the total solid requires

$$\phi_t = \phi_s + \overline{c}(1 - \phi_s), \tag{23}$$

where ϕ_s is the solid volume fraction enclosed by the surface and ϕ_t would be the solid volume fraction if none of the solid were dissolved. Eliminating $\overline{c} = c_{\text{eq}}(\overline{H})$ from Eq. (23) using Eq. (22) shows that ϕ_s is very insensitive to the value of $\overline{H}$,

$$\left|\frac{d\log\phi_s}{d\log\overline{H}}\right| \approx \frac{2c_{\text{sat}}(1-\phi_t)}{\phi_s(1-c_{\text{sat}})^2}\frac{\nu_m\sigma|\overline{H}|}{kT} \ll 1, \tag{24}$$

where we have used Eq. (5). Thus, in a "perfect closed" system, we take ϕ_s constant, which is an excellent approxi-

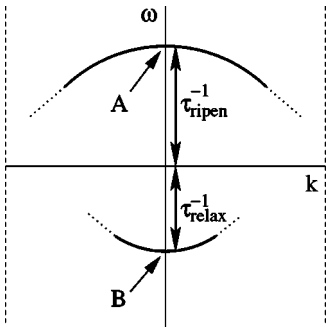

FIG. 4. The spectrum of eigenvalues ω of the operator $\mathcal{L}$ controls the instability of the CMC surfaces under both open and closed system dynamics. There must be an unstable mode at $k=0$, indicated by point *A*, but this mode is suppressed under closed system dynamics by conservation of solid volume, since the next mode at $k=0$, indicated by point *B*, is stable. The dashed lines indicate the Brillouin zone boundaries.

mation for $\tau > \tau_{\text{pore}}$. This dynamics is now given by Eq. (8) with the constant $H^\star$ replaced by $\overline{H}$, whose evolution with time is controlled by the constraint of constant $\phi_s \approx (\phi_t - c_{\text{sat}})/(1-c_{\text{sat}})$. This is surface area minimization under the constraint that the volume contained within the surface is conserved.

Consider again periodic surfaces of the Anderson type. Figure 3(b) shows the total surface area as a function of ϕ_s along the manifold of CMC surfaces of simple cubic structure. Although all CMC solutions represent fixed points of the dynamics, we anticipate that for a given ϕ_s, only the CMC surface with the lowest area can be stable under these dynamics, and then only if the system is also required to maintain its spatial periodicity. We have confirmed this by direct simulation using SURFACE EVOLVER [13,16]—the surfaces along the lower energy branch in Fig. 3(b) are selected by surface area minimization at constant volume provided one works with one unit cell of the Anderson surfaces with periodic boundary conditions. This result is an extension of the well-known stability of the minimal surface (point *M* in Fig. 3) to the entire lower branch in Fig. 3(b), under periodic surface area minimization dynamics with conserved volume.

A corollary of this result is that along this lower branch $\mathcal{L}$ or equivalently $\mathcal{H}$ has only one unstable $k=0$ mode, which is disallowed by solid conservation under closed system dynamics. Thus the eigenmode spectrum of $\mathcal{H}$, outlined in Eq. (20), has the band structure shown in Fig. 4; at small k there can only be one unstable branch of the spectrum. For a unit cell system with periodic boundary conditions, only the $k=0$ modes can participate in the dynamics, and the instability is suppressed by the volume conservation. Thus the stable mode with the longest relaxation time τ_{relax} will control approach to the stable CMC surface; dimensional analysis suggests that $\tau_{\text{relax}} \sim \tau_{\text{ripen}}$ (cf. Fig. 4).

Nevertheless, for an extended system this apparent stability is compromised by the unstable hydrodynamic ($k \neq 0$) modes in the eigenvalue spectrum Eq. (20), which do conserve the overall ϕ_s. It is possible for these unstable modes to be restricted to the topmost ($n=0$) band and to wave vectors $k < \pi/\ell_0$, such that transport of solute over length scales $> \ell_0$ is needed to activate these modes. For amorphous surfaces, the band structure picture is not appropriate, but we still expect unstable modes to appear above a characteristic length scale $\ell_0 \gtrsim L$. In either case, it is natural to ask if there is a window of time over which the CMC surfaces might be observable, before the instability manifests itself.

During the time τ_{relax} characterizing the relaxation to the CMC surface, the diffusion length over which solid transport is possible is $\ell_D = \sqrt{D\tau_{\text{relax}}}$. Using the reaction-limited constraint $D \gg K_f L/c_{\text{sat}}$ and $\tau_{\text{relax}} \sim \tau_{\text{ripen}}$, with τ_{ripen} given by Eq. (19), we find

$$\frac{\ell_D}{L} \gg \sqrt{\frac{kTL}{\sigma \nu_m c_{\text{sat}}}} \gg 1, \tag{25}$$

where the last inequality follows from Eq. (5), and $c_{\text{sat}} \leqslant 1$. Since we thus expect $\ell_D \gg \ell_0$, by the time a surface relaxes on the pore scale to a CMC surface, the diffusive transport between pores will have activated the unstable dynamics, taking the system away from this surface. Thus we do not expect an intermediate-time window over which CMC surfaces would be seen [14].

VI. CONCLUSION AND GEOPHYSICAL EXAMPLES

Our primary result is a kind of "no-go" theorem: CMC surfaces will in practice be rather irrelevant to the surface-tension-driven ripening of porous media, at least in the single-component case studied here. Thus we expect that long-time behavior of such media to be dominated by ripening through a variety of structures that do not necessarily have any resemblance at all to CMC surfaces. It remains only to specify the time scale over which the ripening phenomena will become dominant.

Using representative values for K_f and σ for quartz in water [15], we get for $L \sim 100$ μm that $\tau_{\text{ripen}} \sim 500 \times 10^6$ yr, a time scale over which a geological system should be regarded as open. However, a similar estimate for $CaCO_3$ yields a value of $\tau_{\text{ripen}} \sim 7$ yr, which is quite short on geological time scales. On this time scale, the concentration of solute in the water is determined by conservation of the total amount of the solid components, characteristic of a closed system [17].

Finally, for the example of a crushed ice pack with air as the interstitial fluid, we have over the range -10 to $0\,^\circ$C that K_f increases from 6×10^{-5} to 1.3×10^{-4} m/s. For a packing of grains with a 1.5 mm diameter and a surface energy for the ice of $\sigma = 109$ mN/m, this yields estimates for ripening times in the range 26 to 57 days.

ACKNOWLEDGMENTS

We would like to thank I. Androulakis, P. Chaikin, S. Milner, and T. Witten for helpful and informative discussions. A. Herhold and R. Polizzotti advised us on the properties of real sedimentary materials. K. Brakke assisted us with questions regarding the use of the *surface evolver* software. We are grateful to F. Leyvraz for pointing out an error in our reasoning, and to M. Hastings for bringing to our attention the "gauge" transformation used in Ref. [13].

APPENDIX

A. Basic differential geometry, notations and definitions

Consider a surface $\mathbf{X}(u,v)$. The unit normal to the surface at any point P is denoted by $\mathbf{N}(u,v)$. A complete local description of the surface is given by the distance between neighboring points ds as functions of du and dv and the projection κ_n of the curvature vector of a curve in a direction du/dv onto the normal $\mathbf{N}$,

$$ds^2 = Edu^2 + 2Fdu\ dv + G\ dv^2, \tag{A1}$$

$$\kappa_n = \frac{edu^2 + 2fdudv + gdv^2}{Edu^2 + 2Fdudv + Gdv^2}. \tag{A2}$$

Equation (A1) is the first fundamental form, while Eq. (A2) gives the ratio of the second to the first fundamental form.

The coefficients E,F,G,e,f,g depend on the coordinates and change from one coordinate system to another. They can be defined in terms of the tangent vectors $\mathbf{X}_u,\mathbf{X}_v$ and the normal $\mathbf{N}$ by

$$E = \mathbf{X}_u \cdot \mathbf{X}_u, \quad F = \mathbf{X}_u \cdot \mathbf{X}_v, \quad G = \mathbf{X}_v \cdot \mathbf{X}_v, \tag{A3}$$

$$e = -\mathbf{X}_u \cdot \mathbf{N}_u, \quad f = -\frac{1}{2}(\mathbf{X}_u \cdot \mathbf{N}_v + \mathbf{X}_v \cdot \mathbf{N}_u),$$

$$g = -\mathbf{X}_v \cdot \mathbf{N}_v. \tag{A4}$$

A special coordinate system is defined by the principal directions of the curvature. That is, at each point the tangent vector $\mathbf{X}_u$ points to the direction of maximal curvature and the other tangent vector $\mathbf{X}_v$ points to the direction of minimal curvature. One can show that this is the only coordinate system for which both off-diagonal terms F,f vanish at each point on the surface. Moreover, using this coordinate system one can show that

$$\kappa_1 = e/E, \tag{A5}$$

$$\kappa_2 = g/G. \tag{A6}$$

At any given point on the surface one can define the mean curvature $H(u,v)$ as the average of the two principal curvatures, $\kappa_1(u,v)$ and $\kappa_2(u,v)$. The Gaussian curvature $K(u,v)$ is the product of $\kappa_1(u,v)$ and $\kappa_2(u,v)$. In terms of E,F,G,e,f,g:

$$H = \frac{Eg - 2fF + Ge}{2(EG - F^2)}, \tag{A7}$$

$$K = \frac{eg - f^2}{EG - F^2}. \tag{A8}$$

The coefficients E,F,G,e,f,g cannot be arbitrary smooth differentiable functions of u and v, but must satisfy the Gauss and Gauss-Codazzi equations

$$K = -\frac{1}{\sqrt{EG}}\left[\frac{\partial}{\partial u}\left(\frac{1}{\sqrt{E}}\frac{\partial\sqrt{G}}{\partial u}\right) + \frac{\partial}{\partial v}\left(\frac{1}{\sqrt{G}}\frac{\partial\sqrt{E}}{\partial v}\right)\right] \tag{A9}$$

and

$$\frac{\partial\kappa_1}{\partial v} = \frac{1}{2}(\ln E)_v(\kappa_2 - \kappa_1),$$

$$\frac{\partial\kappa_2}{\partial u} = \frac{1}{2}(\ln G)_u(\kappa_1 - \kappa_2). \tag{A10}$$

The second derivatives of the tangent vectors $\mathbf{X}_{uu},\mathbf{X}_{uv},\mathbf{X}_{vv}$ can be expressed in terms of the local coordinate system $\mathbf{X}_u,\mathbf{X}_v,\mathbf{N}$ by using the Christoffel symbols

$$\mathbf{X}_{uu} = \Gamma^1_{11}\mathbf{X}_u + \Gamma^2_{11}\mathbf{X}_v + e\mathbf{N},$$

$$\mathbf{X}_{uv} = \Gamma^1_{12}\mathbf{X}_u + \Gamma^2_{12}\mathbf{X}_v + f\mathbf{N},$$

$$\mathbf{X}_{vv} = \Gamma^1_{22}\mathbf{X}_u + \Gamma^2_{22}\mathbf{X}_v + g\mathbf{N}. \tag{A11}$$

In the special coordinate system that we chose the Christoffel symbols are

$$\Gamma^1_{11} = \frac{1}{2}\frac{E_u}{E}, \quad \Gamma^2_{11} = -\frac{1}{2}\frac{E_v}{G},$$

$$\Gamma^1_{12} = \frac{1}{2}\frac{E_v}{E}, \quad \Gamma^2_{12} = \frac{1}{2}\frac{G_u}{G},$$

$$\Gamma^1_{22} = -\frac{1}{2}\frac{G_u}{E}, \quad \Gamma^2_{22} = \frac{1}{2}\frac{G_v}{G}. \tag{A12}$$

We need also the surface derivatives of the normal $\mathbf{N}$:

$$\mathbf{N}_u = \frac{fF - eG}{EG - F^2}\mathbf{X}_u + \frac{eF - fE}{EG - F^2}\mathbf{X}_v,$$

$$\mathbf{N}_v = \frac{gF - fG}{EG - F^2}\mathbf{X}_u + \frac{fF - gE}{EG - F^2}\mathbf{X}_v. \tag{A13}$$

B. Linear expansion

Here we will calculate the perturbed mean curvature from Eqs. (A3) and (A4). Let us represent the perturbed surface by the same coordinate system that was chosen for the unperturbed surface. That is,

$$\mathbf{X}'(u,v) = \mathbf{X}(u,v) + \epsilon(u,v)\mathbf{N}(u,v), \tag{A14}$$

where the coordinate system (u,v) is chosen such that the tangents $\mathbf{X}_u,\mathbf{X}_v$ are the principal directions of curvature at any point of the unperturbed surface $\mathbf{X}(u,v)$.

From Eq. (A14) we get

$$\mathbf{X}'_u = \mathbf{X}_u + \epsilon\mathbf{N}_u + \epsilon_u\mathbf{N}, \tag{A15}$$

$$\mathbf{X}'_v = \mathbf{X}_v + \epsilon\mathbf{N}_v + \epsilon_v\mathbf{N}. \tag{A16}$$

We will need also the normal to the perturbed surface $\mathbf{N}'$. To obtain it we use the fact that $\mathbf{X}_u,\mathbf{X}_v,\mathbf{N}$ form an orthogonal system and write

$$\mathbf{N}' = \alpha\mathbf{N} + \beta\mathbf{X}_u + \gamma\mathbf{X}_v, \tag{A17}$$

where α, β, γ are determined by requiring $\mathbf{N}'$ to be a unit vector orthogonal to the two tangents vectors of the perturbed surface:

$$\mathbf{N}'\mathbf{X}_u' = \mathbf{N}'\mathbf{X}_v' = 0, \tag{A18}$$

$$\alpha^2 + E\beta^2 + G\gamma^2 = 1. \tag{A19}$$

We find, to leading order in ϵ,

$$\mathbf{N}' = \mathbf{N} - \frac{\epsilon_u}{E}\mathbf{X}_u - \frac{\epsilon_v}{G}\mathbf{X}_v. \tag{A20}$$

In order to calculate the coefficients of the first and second fundamental forms of the perturbed surface we have to know also the derivatives $\mathbf{N}_u'$ and $\mathbf{N}_v'$. Now we use Christoffel symbols (A11) to express the second derivatives $\mathbf{X}_{uu}, \mathbf{X}_{vv}, \mathbf{X}_{uv}$ in terms of $\mathbf{X}_u, \mathbf{X}_v, \mathbf{N}$. We find

$$\mathbf{N}_u' = -\frac{e}{E}\mathbf{X}_u - \left(\frac{\epsilon_u}{E}[\Gamma_{11}^1\mathbf{X}_u + \Gamma_{11}^2\mathbf{X}_v + e\mathbf{N}] + \frac{\epsilon_{uu}}{E}\mathbf{X}_u - \frac{\epsilon_u E_u}{E^2}\mathbf{X}_u\right) - \left(\frac{\epsilon_v}{G}[\Gamma_{12}^1\mathbf{X}_u + \Gamma_{12}^2\mathbf{X}_v] + \frac{\epsilon_{vu}}{G}\mathbf{X}_v - \frac{\epsilon_v G_u}{G^2}\mathbf{X}_v\right).$$

Reorganizing the above expression, we find

$$\mathbf{N}_u' = \mathbf{X}_u\left[-\frac{e}{E} - \frac{\epsilon_u}{E}\Gamma_{11}^1 - \frac{\epsilon_{uu}}{E} + \frac{\epsilon_u E_u}{E^2} - \frac{\epsilon_v}{G}\Gamma_{12}^1\right] + \mathbf{X}_v\left[-\frac{\epsilon_u}{E}\Gamma_{11}^2 - \frac{\epsilon_v}{G}\Gamma_{12}^2 - \frac{\epsilon_{vu}}{G} + \frac{\epsilon_v G_u}{G^2}\right] - \frac{e}{E}\epsilon_u\mathbf{N}. \tag{A21}$$

We use the Christoffel symbols in the above expression for $\mathbf{N}_u'$ and find

$$\mathbf{N}_u' = \mathbf{X}_u\left[-\frac{e}{E} + \frac{1}{2}\frac{E_u}{E^2}\epsilon_u - \frac{1}{2}\frac{E_v}{EG}\epsilon_v - \frac{\epsilon_{uu}}{E}\right] + \mathbf{X}_v\left[\frac{1}{2}\frac{E_v}{EG}\epsilon_u - \frac{1}{2}\frac{G_u}{G^2}\epsilon_v - \frac{\epsilon_{uv}}{G}\right] - \frac{e}{E}\epsilon_u\mathbf{N}. \tag{A22}$$

A similar expression for $\mathbf{N}_v'$ is obtained by replacing $u \leftrightarrow v$ and $G \leftrightarrow E$ in the above expression:

$$\mathbf{N}_v' = \mathbf{X}_v\left[-\frac{g}{G} + \frac{1}{2}\frac{G_v}{G^2}\epsilon_v - \frac{1}{2}\frac{G_u}{EG}\epsilon_u - \frac{\epsilon_{vv}}{G}\right] + \mathbf{X}_u\left[\frac{1}{2}\frac{G_u}{EG}\epsilon_v - \frac{1}{2}\frac{E_v}{E^2}\epsilon_u - \frac{\epsilon_{uv}}{E}\right] - \frac{g}{G}\epsilon_v\mathbf{N}. \tag{A23}$$

Substituting Eqs. (A15), (A16), (A20), (A22), and (A23) in Eqs. (A3) and (A4) we obtain the coefficients of the first and second fundamental forms of the perturbed surface [in the coordinate system (A14)]:

$$E' = E - 2\epsilon e + O(\epsilon^2),$$

$$G' = G - 2\epsilon g + O(\epsilon^2),$$

$$F' = O(\epsilon^2),$$

$$e' = e - \epsilon\frac{e^2}{E} - \frac{1}{2}\frac{E_u}{E}\epsilon_u + \frac{1}{2}\frac{E_v}{G}\epsilon_v + \epsilon_{uu} + O(\epsilon^2),$$

$$g' = g - \epsilon\frac{g^2}{G} - \frac{1}{2}\frac{G_v}{G}\epsilon_v + \frac{1}{2}\frac{G_u}{E}\epsilon_u + \epsilon_{vv} + O(\epsilon^2),$$

$$f' = \frac{1}{2}\frac{E_v}{E}\epsilon_u - \frac{1}{2}\frac{G_u}{G}\epsilon_v + \epsilon_{uv} + O(\epsilon^2). \tag{A24}$$

The existence of $O(\epsilon)$ corrections to the off-diagonal term f' of the second fundamental form indicates that the coordinate system we chose is not (to linear order in the perturbation) along the principal directions of the perturbed surface. However, the absence of $O(\epsilon)$ terms in F' indicates that the coordinate system is still orthogonal (to linear order in ϵ).

Substituting the perturbed coefficients (A24) into Eq. (A7) we arrive at the following linear expansion of the mean curvature:

$$H = H^\star + \frac{1}{2}\epsilon\left(\frac{g^2}{G^2} + \frac{e^2}{E^2}\right) + \frac{1}{4E}\left(\frac{G_u}{G} - \frac{E_u}{E}\right)\epsilon_u + \frac{1}{4G}\left(\frac{E_v}{E} - \frac{G_v}{G}\right)\epsilon_v + \frac{1}{2E}\epsilon_{uu} + \frac{1}{2G}\epsilon_{vv}. \tag{A25}$$

Moreover, using Eqs. (A5) and (A6) and the Codazzi equations, the above equation can be recast in the form

$$H = H^\star + \epsilon(2H^{\star 2} - K) + \frac{1}{2}\left\{\epsilon_u\frac{1}{2E}[\ln(G/E)]_u + \epsilon_v\frac{1}{2G}[\ln(E/G)_v]\right\} + \frac{1}{2E}\epsilon_{uu} + \frac{1}{2G}\epsilon_{vv}. \tag{A26}$$

or

$$H = H^\star + \epsilon\frac{1}{2}(\kappa_1{}^2 + \kappa_2{}^2) + \frac{1}{2(\kappa_1 - \kappa_2)}[D_u\kappa_2 D_u\epsilon - D_v\kappa_1 D_v\epsilon] + \frac{1}{2}[D^2{}_u\epsilon + D^2{}_v\epsilon], \tag{A27}$$

where in the above equation we introduced the covariant derivatives

$$D_u \equiv \frac{1}{\sqrt{E}}\partial_u, \quad D_v \equiv \frac{1}{\sqrt{G}}\partial_v. \tag{A28}$$

On a CMC we have $D_u\kappa_1 = -D_u\kappa_2, D_v\kappa_1 = -D_v\kappa_2$. This implies the relation

$$\frac{1}{(\kappa_1 - \kappa_2)}[D_u\kappa_2 D_u\epsilon - D_v\kappa_1 D_v\epsilon] = \frac{1}{(\kappa_1 - \kappa_2)}[D_u\kappa_2 D_u\epsilon + D_v\kappa_2 D_v\epsilon] = \frac{\boldsymbol{\nabla}_s\kappa_2 \cdot \boldsymbol{\nabla}_s\epsilon}{(\kappa_1 - \kappa_2)},$$

where $\boldsymbol{\nabla}_s$ is a projection of the gradient on the surface $\mathbf{X}(u,v)$:

$$\nabla_s \equiv \frac{\mathbf{X}_u \partial_u}{|\mathbf{X}_u|^2} + \frac{\mathbf{X}_v \partial_v}{|\mathbf{X}_v|^2}. \tag{A29}$$

Also we have

$$\nabla_s K = \nabla_s(\kappa_1 \kappa_2) = (\kappa_1 - \kappa_2)\nabla_s \kappa_2,$$

which leads to

$$\nabla_s \kappa_2 = \frac{\nabla_s K}{\kappa_1 - \kappa_2}.$$

Also,

$$(\kappa_1 - \kappa_2)^2 = 4(H^{\star 2} - K).$$

So finally we obtain, in a coordinate-free form,

$$H = H^* + (2H^{\star 2} - K)\epsilon - \frac{1}{8}\nabla_s \ln(H^{\star 2} - K) \cdot \nabla_s \epsilon + \frac{1}{2}\nabla_s{}^2 \epsilon. \tag{A30}$$

[1] A. J. Bray, Adv. Phys. **43**, 357 (1994).

[2] I. Lifshitz and V. Slyozov, J. Phys. Chem. Solids **19**, 35 (1961); C. Wagner, Z. ElectroChem. **65**, 581 (1961); P. W. Voorhees, Annu. Rev. Mater. Sci. **22**, 197 (1992).

[3] D. Weaire and S. Hutzler, *The Physics of Foams* (Oxford University Press, Oxford, 1999).

[4] R. de Boer, Geochim. Cosmochim. Acta **41**, 249 (1977).

[5] S. Békri, J. Thovert, and P. Adler, Chem. Eng. Sci. **50**, 2765 (1995).

[6] G. Daccord, O. Liétard, and R. Lenormand, Chem. Eng. Sci. **48**, 179 (1993).

[7] E. Thomas, D. Alward, D. Kinning, D. Martin, J. Handlin, and L. Fetters, Macromolecules **19**, 2197 (1986).

[8] http://www.msri.org/publications/sgp/SGP/.

[9] J. C. Nitsche, *Lectures on Minimal Surfaces* (Cambridge University Press, London, 1999).

[10] J. Sethian, *Level Set Methods and Fast Marching Methods*, 2nd ed. (Cambridge University Press, London, 1999).

[11] D. Anderson, H. Davis, L. Scriven, and J. C. Nitsche, Adv. Chem. Phys. **77**, 337 (1990).

[12] N. Hatano and D. R. Nelson, Phys. Rev. Lett. **77**, 570 (1996).

[13] B. Davidovitch, D. Ertaş, and T. C. Halsey, Philos. Mag. **84**, 1937 (2004).

[14] This is only the case for connected pore spaces. Disconnected pore spaces, e.g., isolated spherical "vugs," can be metastable.

[15] P. Dove, Am. J. Sci. **294**, 665 (1994); R. Iler, *The Chemistry of Silica* (John Wiley and Sons, New York, 1979).

[16] http://www.susqu.edu/facstaff/b/brakke/evolver.

[17] L. Plummer, T. Wigley, and D. Parkhurst, Am. J. Sci. **278**, 179 (1978); J. Mullin, *Crystallization*, 4th ed. (Butterworth-Heinemann, Oxford, 2001).